J. Phys. B: At. Mol. Opt. Phys. **29** (1996) 2543–2552. Printed in the UK

The K- and L-shell ionization of atoms by 1 GeV protons

I B Vodopyanov, V V Pashuk and M V Stabnikov
Radiation Physics Laboratory, Petersburg Nuclear Physics Institute, Gatchina 188350, Russia

Received 5 October 1995

Abstract. Cross sections for K-vacancy and L-x-ray production by 1 GeV protons for elements ranging from Cu to U are measured and compared with calculations based on the plane-wave Born approximation. The analysis revealed the need to include the current–current interaction between the projectile and target electron and the spin-flip term.

1. Introduction

Inner-shell ionization of atoms by ions has been the subject of numerous investigations. Most data of the K- and L-shell vacancy production were obtained for non-relativistic projectiles. Most of them are in agreement with the theory of Brandt and Lapicki (1979, 1981). This theory is a modification of the plane-wave Born approximation (PWBA). It includes corrections for particle energy loss, Coulomb deflection, polarization and binding changes of the electrons in a perturbed stationary state and relativistic effects (ECPSSR).

Only a few measurements have been carried out for projectile energies above 100 MeV per nucleon. Jarvis *et al* (1972) and Anholt *et al* (1976) investigated K-x-ray production by 160 MeV and 4.88 GeV protons. The Brandt and Lapicki (1979, 1981) corrections are not so significant for this energy range. The comparison with PWBA using the Darwin approximation to the relativistic wavefunction indicated that in addition to the ordinary Coulomb interaction between the projectile and atomic electron (longitudinal contribution), the current–current interaction between the two charged particles (transverse contribution) and the spin-flip effect contribute significantly in such a process (Davidovič *et al* 1978, Anholt 1979).

By employing the PWBA and including the direct Coulomb interaction, the interaction between atomic electron and projectile current densities and the spin-flip effect, and describing the K-electron using semirelativistic Darwin functions, Anholt obtained the ionization cross section in the form

$$\sigma_{\mathrm{K}} = \frac{8\pi Z_1^2}{\eta_{\mathrm{K}} Z^4} \int_{W_{\min}}^{\infty} d^2 \, \mathrm{d}W \int_{Q_{\min}}^{\infty} \frac{\mathrm{d}Q}{Q^2} \left(F_{\mathrm{K}} + \frac{(\beta Z\alpha)^2 (1 - Q_{\min}/Q)}{(1 - \beta^2 Q_{\min}/Q)^2} \left(G_{\mathrm{K}} + \frac{Q F_{\mathrm{K}}}{4} \right) \right) \qquad (1)$$

where

$$d^2 = (1 + (Z\alpha/2)^2)^{-1} (1 + (W-1)(Z\alpha/2)^2)^{-1}$$
$$W_{\min} = 2U_{\mathrm{K}}/Z^2 \qquad Q_{\min} = W^2/4\eta_{\mathrm{K}}$$
$$\eta_{\mathrm{K}} = v^2/Z^2 \qquad Z = Z_2 - 0.3$$

where U_{K} is the K-electron binding energy, v the projectile velocity, Z_1 the projectile charge, Z_2 the target charge, and F_{K} and G_{K} are essentially the non-relativistic matrix elements

$$F_{\mathrm{K}} = (3Q + W) Q A_3 \qquad G_{\mathrm{K}} = W A_2/4$$

0953-4075/96/122543+10$19.50

with

$$A_n = \frac{2^7 \exp(-2/k \tan^{-1}(2k/(Q+1-k^2)))}{3(1-\exp(-2\pi/k))((Q-k^2+1)^2+4k^2)^n}$$

and

$$k = \sqrt{W-1}\,.$$

The investigations of K- and L-x-ray production by relativistic heavy ions (Anholt *et al* 1977, 1984) showed the importance of these contributions both for K- and for L-shell ionization calculations. L-x-ray production data obtained by Anholt *et al* (1984) are the only ones for relativistic projectiles.

Rustgi *et al* (1988) have compared the calculations for the K-shell of Anholt (1979) to the calculations using Dirac–Hartree–Fock-type wavefunctions in the PWBA and the Dirac–hydrogenic-type wavefunctions in the semiclassical approximation. They concluded that an accurate description of the projectile–target interaction is far more important than improving the accuracy of the wavefunction being used.

We found that obtaining additional data for inner-shell vacancy production by relativistic projectiles is pertinent. The present paper outlines the experimental set-up and examines the experimental data for K- and L-shell ionization by 1 GeV protons.

2. Experiment

The experimental geometry is shown in figure 1. The 1 GeV proton beam from the Petersburg Nuclear Physics Institute synchrocyclotron was focused onto the target by three pairs of quadrupoles to form a spot of about 1 cm diameter. After emerging from the evacuated target chamber the proton beam passed through a beam monitor. The target chamber was constructed so that the targets were observed by the x-ray detector at an angle of 135° to the beam direction. This disposition served for reducing the intensity of protons scattered by the target which might pass through the detector. Because of the high background the detector was covered with 10 cm lead protection with a 1 cm diameter window.

The monitor was an air-filled ionization chamber placed downstream of the target. It was coupled to the integrator to integrate the relative intensity of the beam for 10 s

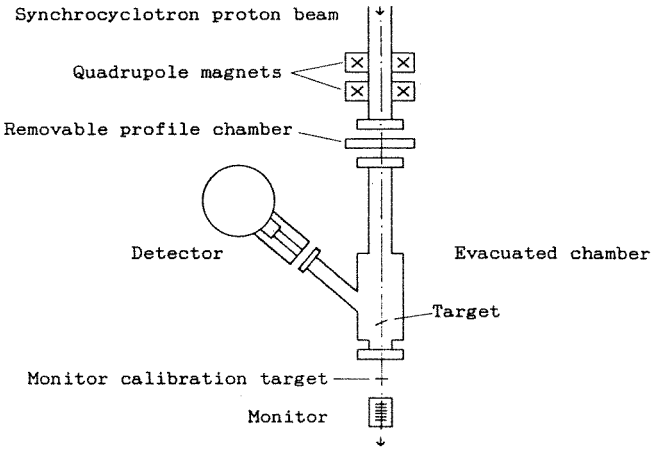

Figure 1. General layout of the experimental apparatus.

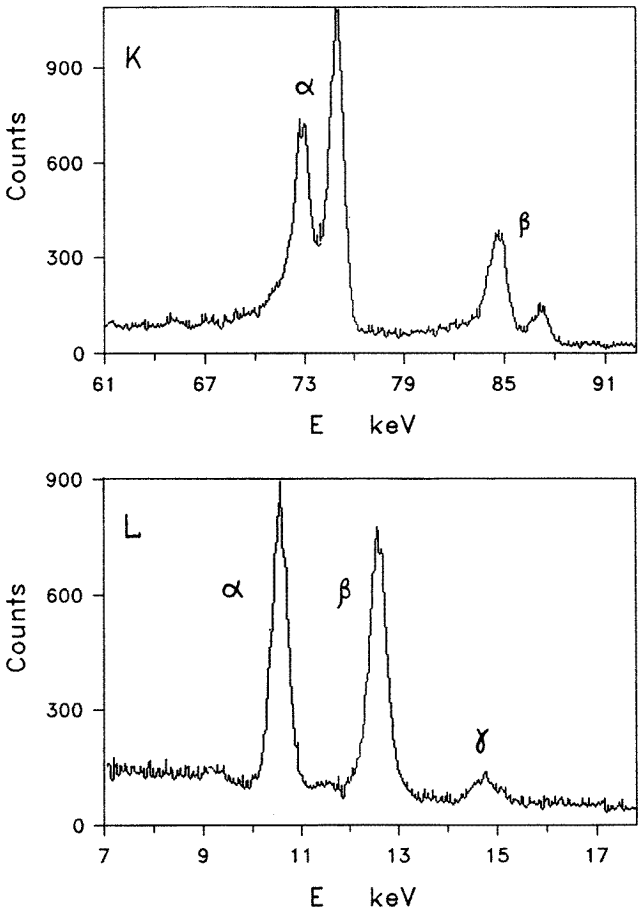

Figure 2. X-ray spectra for the Pb target.

cycles (Lobanov and Stabnikov 1983). The absolute intensity of the beam was found by irradiation of a 2 mm thick graphite target. The annihilation radiation from the β^+ decay of ^{11}C formed in the reaction ^{12}C(p, pn) ^{11}C was measured off-line. The monitoring error of 5% was mainly due to the uncertainty of known reaction cross sections for 1 GeV protons (Cumming 1963).

Two detectors were used: a Si(Li) spectrometer for x-ray energies ranging from 4 to 30 keV or a Ge(Li) spectrometer for x-ray energies ranging from 20 to 120 keV. The energy resolution was 0.4 keV at 25 keV for Si(Li) and 0.7 keV at 95 keV for Ge(Li). Typical x-ray pulse height spectra are shown in figure 2. The detector efficiencies versus energy were determined using ^{241}Am, ^{57}Co, ^{54}Mn, ^{152}Eu, ^{133}Ba, ^{137}Cs, ^{139}Ce and ^{109}Cd calibrated sources assuming the γ-ray and x-ray yields quoted by Holnov *et al* (1980) and Chechev *et al* (1988). In the calibration procedure, radiation absorption by air and source cover were taken into account. Generally, the detector efficiency uncertainty was about 3% due to yield uncertainties of the sources for energy range between 5 and 120 keV.

To make dead-time corrections a pulser was fed into the detector. The corrections were determined for every spectrum using the integrated pulser peak counting rate; they amounted to 3–20%.

The amplified signals from the detector were fed into a CAMAC-based spectrum analyser

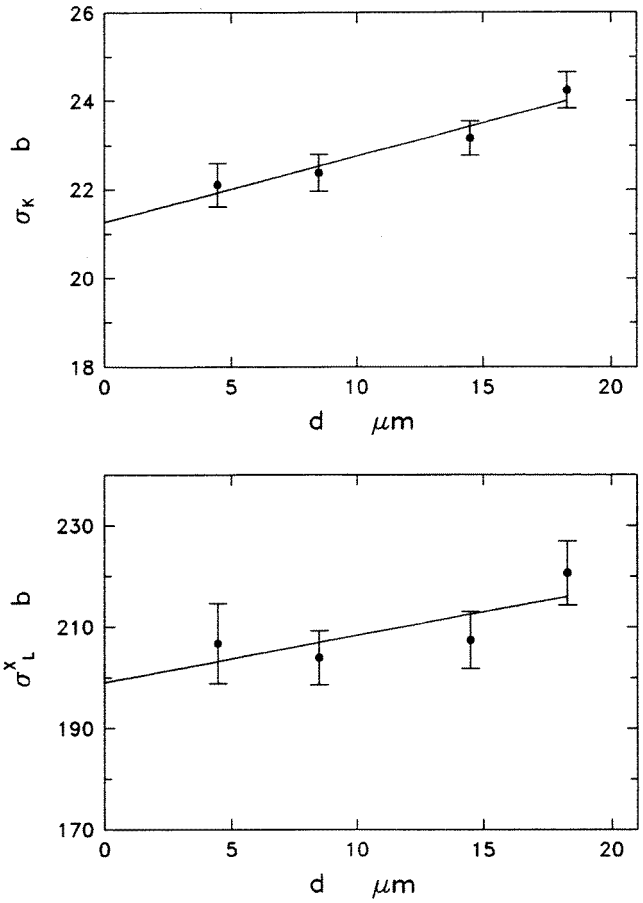

Figure 3. Dependence of the measured Tb cross section on target thickness. Corrections to the original data were made by extrapolation to zero thickness.

coupled to the IBM PC. The software permitted set-up operation, data reduction, graph plotting and data storage. To determine peak areas of x-ray spectra, a special algorithm was used (Kabina *et al* 1982). The program based on this algorithm permitted us to fit asymmetric overlapping peaks on a background continuum, by the least-squares method. The peaks were Gaussians with asymmetrizing additions; the background was a polynomial plus a smooth step for every peak. A definite energy could be attributed to every peak.

When obtaining the x-ray cross sections one took into account the target self-absorption, absorption in the chamber mylar window (50 μm thick) and that in the air between the chamber window and detector window (see figure 1).

The targets were as follows: self-supporting Cu, Zr, Cd, Tb, Ta and Pb foils (thickness between 5 and 20 μm). Pb and Bi (3–4 μm) prepared by vacuum evaporation onto a 15 μm mylar backing and uranium oxide painted onto an Al foil (effective U thickness: 1 μm). Target thicknesses were estimated by weighing with an average uncertainty of 2%. Since secondary particles increase the yield in thicker targets (see Jarvis *et al* 1972, Anholt *et al* 1976, 1984), the cross section was corrected by using targets of several thicknesses for every element (except Bi and U), and by extrapolating the cross section to zero thickness (see the two examples in figure 3). Even though the slope could be zero in the lower part of the figure, we used the slope determined by least squares in all cases.

The total experimental cross section errors include the components as follows: the

monitoring error; the detector efficiency error; statistics errors; the set-up geometry errors; the errors due to the x-ray absorption corrections; the errors of the target thickness correction, given by standard least-squares minimization procedure.

3. K-shell ionization data

The K-shell experimental data for 1 GeV protons are listed in table 1 and are presented graphically in figure 4. To determine the total ionization cross sections from the x-ray production cross sections we used the fluorescent yield ω_K obtained by Bambynek *et al* (1972). The full curve is derived from the calculations based on the formalism by Anholt (1979), equations (1).

We failed to obtain ionization cross section for uranium because the K-x-ray yield was insufficient due to both small σ_K and the thinness of the U target, and the signal-to-background ratio was small too.

The calculated cross sections are in good agreement with experiment, except possibly for the high-Z targets.

Table 1. Experimental K-shell ionization cross sections in barns for 1 GeV incident protons as a function of atomic number. The errors are given in units of the last digit.

Element	Z	σ_K (expt)
Cu	29	186(13)
Zr	40	83.1(78)
Cd	48	45.5(40)
Tb	65	22.2(15)
Ta	73	16.6(14)
Pb	82	10.5(7)
Bi	83	10.4(8)

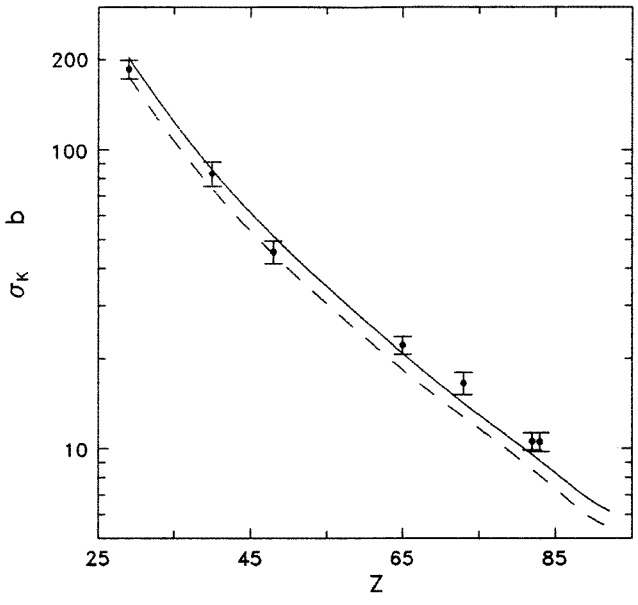

Figure 4. K-shell ionization cross sections for 1 GeV proton projectiles. The full curve is derived from the calculations based on the formalism by Anholt (1979). The chain curve is the longitudinal Coulomb contribution in PWBA theory.

To display the non-Coulomb contribution to K-shell ionization we calculated σ_K due to direct Coulomb interaction using the tabulations of Benka and Kropf (1978). The cross section is given by the formula

$$\sigma_S = 8\pi a_0^2 Z_S^{-4} \theta^{-1} F_S(\eta_S/\theta_S^2, \theta_S) \tag{2}$$

where a_0 is the Bohr radius of hydrogen, Z_S is the effective nuclear charge seen by an electron in an inner subshell s. θ_S and η_S are scaled target binding energy and scaled projectile velocity accordingly. The results are plotted in figure 4 as a chain curve. The non-Coulomb contribution to K-shell ionization cross sections is about 15%.

4. L-shell ionization data

L_α, L_β and L_γ x-ray production cross sections for 1 GeV protons were measured for targets ranging from Tb to U. $L_{\gamma 1}$ and L_ℓ lines were extracted for a few targets with significant error. The extraction of other L-lines proved to be impossible due to the poor energy resolution of Si(Li) detector and the intense continuum background. The results are listed in table 2 and are presented graphically in figure 5.

The x-ray production cross sections for the most commonly resolved L_α, L_β and L_γ series peaks are related to the three ionization cross sections σ_{L_1}, σ_{L_2} and σ_{L_3} in the standard way:

$$\sigma^x_{L_\alpha} = (\sigma_{L_1}(f_{12}f_{23} + f_{13}) + \sigma_{L_2} f_{23} + \sigma_{L_3})\omega_3 S_{\alpha 3} \tag{3}$$

$$\sigma^x_{L_\beta} = \sigma_{L_1}(\omega_1 S_{\beta 1} + \omega_2 f_{12} S_{\beta 2} + \omega_3(f_{13} + f_{12}f_{23})S_{\beta 3}) + \sigma_{L_2}(\omega_2 S_{\beta 2} + \omega_3 f_{23} S_{\beta 3}) + \sigma_{L_3}\omega_3 S_{\beta 3} \tag{4}$$

$$\sigma^x_{L_\gamma} = \sigma_{L_1}(\omega_1 S_{\gamma 1} + \omega_2 f_{12} S_{\gamma 2}) + \sigma_{L_2}\omega_2 S_{\gamma 2} \tag{5}$$

$$\sigma^x_{L_{tot}} = \nu_1\sigma_{L_1} + \nu_2\sigma_{L_2} + \nu_3\sigma_{L3} \tag{6}$$

$$\sigma^x_{L_{\gamma 1}} = \sigma_{L_1}\omega_2 f_{12} S_{\gamma 12} + \sigma_{L_2}\omega_2 S_{\gamma 12} \tag{7}$$

where

$$\nu_1 = \omega_1 + f_{12}\omega_2 + (f_{13} + f_{13}f_{12})\omega_3 \qquad \nu_2 = \omega_2 + f_{23}\omega_3 \qquad \nu_3 = \omega_3$$

and S_{ji} ($j = \alpha, \beta, \gamma, \ldots$ and $i = 1, 2, 3$) are the emission rates, ω_i are the fluorescent yields and $f_{ii'}$ are the Coster–Kronig transition rates.

The accuracy of these values greatly affects the result of comparing the experimental data with calculations. ω_i and $f_{ii'}$ were taken from the semiempirical fits of Krause (1979). The uncertainties given are generally of 5% and reach 20% for some values. There are disagreements between the data of Krause and measurements of other researchers (Werner and Jitschin 1988). S_{ij} were taken from the experimental data of Salem *et al* (1974).

Table 2. Experimental L-x-ray production cross sections in barns for 1 GeV incident protons as a function of atomic number.

Element	Z	$\sigma_{L_{tot}}$	σ_{L_α}	σ_{L_β}	σ_{L_γ}
Tb	65	197(13)	99.4(60)	80.9(49)	13(2)
Ta	73	195(16)	98.9(60)	77.7(56)	14(1)
Pb	82	183(14)	96.5(61)	68.7(48)	12(1)
Bi	83	182(11)	92.1(65)	70.5(44)	12(1)
U	92	160(9)	80.1(63)	64.3(39)	13(1)

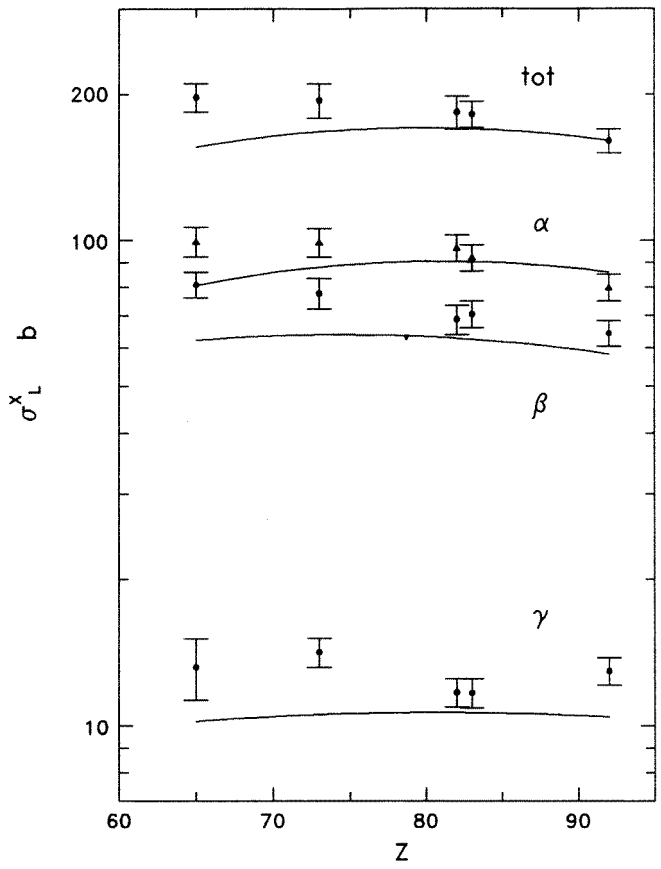

Figure 5. L-shell x-ray production cross sections for 1 GeV proton projectiles. Experimental points for L_α are shown as triangles. The full curve is derived from the PWBA theory including the transverse interaction contribution in the dipole approximation.

The uncertainties given are of 2–8%. The calculated emission rates of Campbell and Wang (1989) are generally in agreement with the data of Salem but for some values differ significantly.

To calculate σ_{L_i} we used formula (2) for longitudinal contribution to L-shell ionization. The formulation of the current–current and spin-flip interactions for L-shell has not been done. We used the dipole approximation (Anholt *et al* 1984) to estimate the transverse contribution given by

$$\frac{\sigma_{\text{tot}}}{\sigma_{\text{long}}} = 1 + \frac{\ln(\gamma^2) - \beta^2}{\ln(E_{\max}/U\gamma^2)} \tag{8}$$

where $E_{\max} = 2mc^2\gamma^2\beta^2$, U is the relevant electron binding energy, and γ and β are projectile relativistic energy and velocity parameters.

The full curve in figure 5 is derived from the calculations for σ_{L_i} using equations (3)–(6). The non-Coulomb correction factor varies from 1.11 to 1.19.

The disagreements between experimental and calculated L-x-ray cross sections reach 30%. The experimental data are higher than the calculations, possibly due to uncertainties in the emission rates, fluorescent yields and Coster–Kronig coefficients.

Table 3. The semiempirical L-subshell ionization cross sections for 1 GeV incident protons.

Element	Z	σ_{L_1}	σ_{L_2}	σ_{L_3}
Tb	65	225(14)	282(17)	664(40)
Ta	73	145(9)	178(11)	437(28)
Pb	82	91.7(57)	111(7)	287(18)
Bi	83	86.7(53)	105(6)	272(17)
U	92	59.8(48)	71.6(57)	196(16)

We tried to use equations (3)–(7) to solve for the experimentally measured subshell ionization cross sections. The direct extraction of σ_{L_i} using a method based on the intensity of the weak $L_{\gamma 44'}$, $L_{\gamma 23}$ or $L_{\gamma 6}$ lines (Cohen 1984) proved to be impossible due to the poor x-ray energy resolution. Solving the system of equations (3) to (7) for σ_{L_1}, by least-squares minimization, we got high correlation coefficients and, therefore, an unstable solution. That is why we present the semiempirical ionization cross sections as the solution of the system of equations (3) to (7) for σ_{L_1} by substitution of $\sigma_{L_1}(\sigma_{L_{2\,theor}}/\sigma_{L_{1\,theor}})$ for σ_{L_2} and of $\sigma_{L_1}(\sigma_{L_{3\,theor}}/\sigma_{L_{1\,theor}})$ for σ_{L_3} (table 3).

5. Summary

The 1 GeV proton data confirmed that K-shell ionization cross sections induced by relativistic projectiles can be predicted by the relativistic PWBA theory including the interaction between atomic electron and projectile current densities and the spin-flip effect. A slight discrepancy between the experimental data and theory for high-Z region appears, possibly due to the use of the Dirac–hydrogenic-type wavefunctions in the semiclassical approximation (Davidovič *et al* 1978, Anholt 1979).

In figure 6 we present the comparison of the K-shell ionization experimental proton data with calculations for energy range of 5–4880 MeV for several targets. The experimental data were taken partially as averaged empirical data of Paul and Sacher (1989), and also from experimental works of Bissinger *et al* (1972), Pineda and Peisach (1990), Jarvis *et al* (1972), Anholt *et al* (1976) and ours. The 1 GeV uranium point is the result of the extrapolation of the other 1 GeV experimental data. Several experimental σ_K for Ni, Ag and W targets were reduced to Cu, Cd and Ta ones by factors like $(\sigma_K^{Cu}/\sigma_K^{Ni})_{ECPSSR}$ etc, in order to be comparable.

For the low-energy region the cross sections were calculated with the ECPSSR theory of Brandt and Lapicki (1979, 1981) using the tabulation of Rice *et al* (1977). For proton energy higher than 100 MeV we used this tabulation and the approximate formulae for transverse and spin-flip terms to be added (Anholt 1979).

It is worth noting a general agreement between the experimental data and theory for the whole energy range. The 160 MeV data (Jarvis *et al* 1972) are systematically higher than the calculated curves; this can also be seen from figures of Paul and Sacher (1989). The longitudinal Coulomb contribution is demonstrated for U as a chain curve.

The difference between the L-shell experimental x-ray production cross sections for 1 GeV incident protons and calculated ones can reach 30%. Such a discrepancy is typical for L-data (Braziewicz and Braziewicz 1988). Besides an inaccuracy of calculations, the discrepancy arises because of the uncertainties of the emission rates, fluorescent yields and Coster–Kronig transition rates. Derivation of the cross sections with different coefficients can lead to values which differ by more than a factor of two (Braziewicz and Braziewicz 1988).

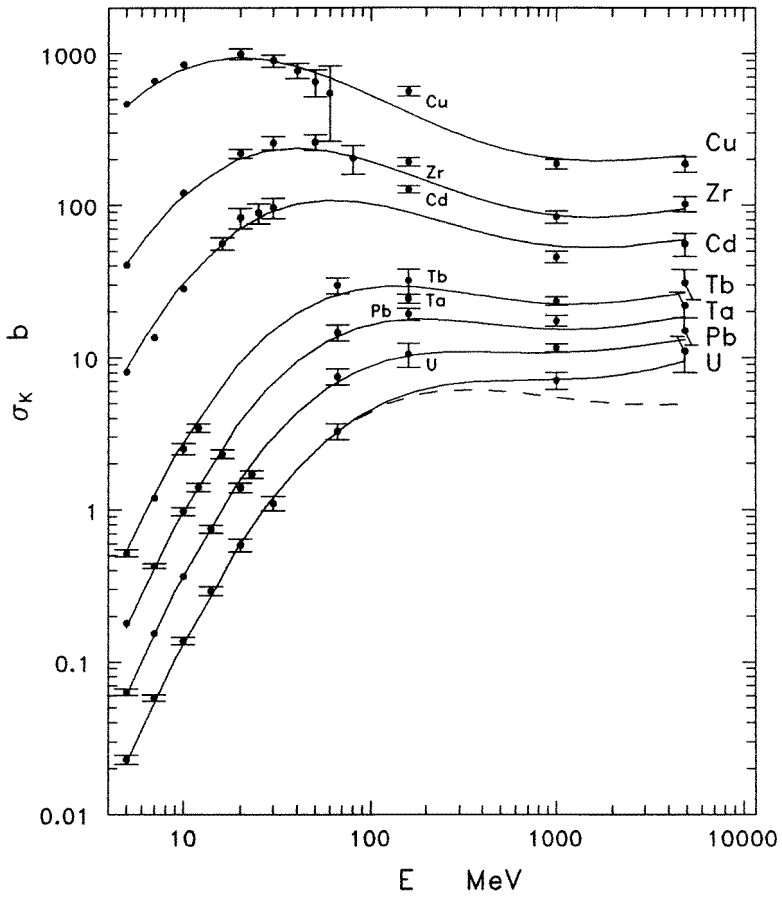

Figure 6. Experimental and theoretical K-shell ionization cross sections for protons versus E_p. The full curve is the ECPSSR cross sections for low energy and calculations according to Anholt (1979) for energy higher than 100 MeV. The chain curve is the PWBA Coulomb contribution for the U target. The 160 MeV data (Jarvis *et al* 1972) are indicated by additional target symbols to be distinguished.

Acknowledgments

We would like to thank Doctors V V Miroshkin, M G Tverskoy and E A Kotikov, and O V Lobanov, V V Lysenko, Z G Medoeva, V U Merculov and A A Tsyganova for help in carrying out the measurements.

References

Anholt R 1979 *Phys. Rev.* A **19** 1004
Anholt R *et al* 1984 *Phys. Rev.* A **30** 2234
Anholt R, Nagamiya S, Rasmussen J O, Bowman H, Ioannou-Yannou J G and Rauscher E 1976 *Phys. Rev.* A **14** 2103
Anholt R, Nagamiya S, Rasmussen J O, Bowman H, Ioannou-Yannou J, Rauscher E, Shibata T and Ejiri H 1977 *Phys. Lett.* **59A** 429

Bambynek W, Crasemann B, Fink R W, Freund H-U, Mark H, Swift C D, Price R E and Venugopala R P 1972 *Rev. Mod. Phys.* **44** 716
Benka O and Kropf A 1978 *At. Data Nucl. Data Tables* **22** 219
Bissinger G A, Shafroth S M and Waltner A W 1972 *Phys. Rev.* A **5** 2046
Brandt W and Lapicki G 1979 *Phys. Rev.* A **20** 465
——1981 *Phys. Rev.* A **23** 1717
Braziewicz E and Braziewicz J 1988 *J. Phys. B: At. Mol. Opt. Phys.* **21** 1537
Campbell J L and Wang J-X 1989 *At. Data Nucl. Data Tables* **43** 281
Chechev V P, Kamynov Sh V, Kuzmenko N K, Sergeev V D and Artamonova K P 1988 *Averaged Nuclear Characteristics of Radioactive Nuclides* (Moscow: Energoatomizdat) (in Russian)
Cohen D D 1984 *J. Phys. B: At. Mol. Phys.* **17** 3913
Cumming J B 1963 *Ann. Rev. Nucl. Sci.* **13** 261
Davidovič D M, Moiseiwitsch B L and Norrington P H 1978 *J. Phys. B: At. Mol. Phys.* **11** 847
Holnov U V, Chechev V P, Kamynov Sh V, Kuzmenko N K and Nedovesov V G 1980 *Radiation Characteristics of Commercial Radioactive Nuclides* (Moscow: Atomizdat) (in Russian)
Jarvis O N, Whitehead C and Shan M 1972 *Phys. Rev.* A **5** 1198
Kabina L P, Kondurov I A and Fedorova E I 1982 *Preprint* Leningrad Nuclear Physics Institute 790
Krause M O 1979 *J. Phys. Chem. Ref. Data* **8** 307
Lobanov O V and Stabnikov M V 1983 *Preprint* Leningrad Nuclear Physics Institute 857
Paul H and Sacher J 1989 *At. Data Nucl. Data Tables* **42** 105
Pineda C A and Peisach M 1990 *Nucl. Instrum. Methods* A **299** 618
Rice R, Basbas G and McDaniel F D 1977 *At. Data Nucl. Data Tables* **20** 503
Rustgi M L, Leung P T and Long S A 1988 *Phys. Rev.* A **37** 3169
Salem S I, Panossian S L and Krause R A 1974 *At. Data Nucl. Data Tables* **14** 91
Werner U and Jitschin W 1988 *Phys. Rev.* A **38** 4009